

NMR Spin-Rotation Relaxation and Diffusion of Methane

P. M. Singer,* D. Asthagiri,† W. G. Chapman, and G. J. Hirasaki

*Department of Chemical and Biomolecular Engineering,
Rice University, 6100 Main St., Houston, TX 77005, USA*

(Dated: March 1, 2018)

The translational-diffusion coefficient D_T and the spin-rotation contribution to the ^1H NMR relaxation time T_{1J} for methane (CH_4) are investigated using MD (molecular dynamics) simulations, over a wide range of densities ρ and temperatures T , spanning the liquid, supercritical, and gas phases. The simulated D_T agree well with measurements, without any adjustable parameters in the interpretation of the simulations. A minimization technique is developed to compute the angular-velocity for non-rigid spherical molecules, which is used to simulate the autocorrelation function $G_J(t)$ for spin-rotation interactions. With increasing D_T (i.e. decreasing ρ), $G_J(t)$ shows increasing deviations from the single-exponential decay predicted by the Langevin theory for hard spheres, and the deviations are quantified using inverse Laplace transforms of $G_J(t)$. T_{1J} is derived from $G_J(t)$ using the kinetic model “ km ” for gases (T_{1J}^{km}), and the diffusion model “ dm ” for liquids (T_{1J}^{dm}). T_{1J}^{km} shows better agreement with T_1 measurements at higher D_T , while T_{1J}^{dm} shows better agreement with T_1 measurements at lower D_T . T_{1J}^{km} is shown to dominate over the MD simulated ^1H - ^1H dipole-dipole relaxation T_{1RT} at high D_T , while the opposite is found at low D_T . At high D_T , the simulated spin-rotation correlation-time τ_J agrees with the kinetic collision time τ_K for gases, from which a new relation $1/T_{1J}^{km} \propto D_T$ is inferred, without any adjustable parameters.

Keywords: Molecular dynamics simulations, Angular velocity, Autocorrelation function, Intramolecular relaxation, Intermolecular relaxation, Hard spheres, Kinetic model

I. INTRODUCTION

Theoretical and experimental investigations into ^1H NMR (nuclear magnetic resonance) spin-rotation relaxation T_{1J} and translational-diffusion D_T of methane (CH_4), deuterio-derivatives ($\text{CH}_{4-n}\text{D}_n$), and halide-derivatives ($\text{CH}_{4-n-m}\text{F}_n\text{Cl}_m$) dates back over 50 years [1–15]. Likewise, the theoretical and experimental investigations into molecular-beam magnetic-resonance of methane and its derivatives dates back over 50 years [16–20], from which came (among many other things) the coupling constants used to interpret T_{1J} .

More recently, the influence of dissolved methane on the T_1 and D_T of complex crude-oils and hydrocarbon mixtures has been investigated [21–24], which reveal the important influence of the spin-rotation contribution from methane. Of particular significance is the well established spin-rotation component for methane in the fast-motion regime [13, 22]:

$$\frac{1}{T_{1J}^A} = A \frac{T^{3/2}}{\rho}, \quad (1)$$

where A is an empirically derived constant. Eq. 1 states that the relaxation rate $1/T_{1J}$ increases with temperature T , i.e. T_{1J} decreases with T . This is in stark contrast to the ^1H - ^1H dipole-dipole relaxation T_{1RT} which increases with T , for all hydrocarbons, including methane. Also of interest recently is the influence of pore confinement on

the NMR response of methane [25–34], which has practical applications for characterizing the light hydrocarbons in the organic nano-pores of kerogen and bitumen in organic-rich shale. One of the current mysteries is why the T_{1S}/T_{2S} ratio for surface-relaxation of methane in organic-shale is typically $T_{1S}/T_{2S} \lesssim 2$, while for higher-order alkanes it is typically higher $T_{1S}/T_{2S} \gtrsim 4$. This has practical applications for separating the NMR response of light hydrocarbon from water in organic-shale, and for determining the hydrocarbon saturation in the organic-shale reservoir.

In order to properly characterize NMR relaxation of methane in the bulk and under nano-pore confinement, one must first separate the ^1H spin-rotation relaxation T_{1J} from ^1H - ^1H dipole-dipole relaxation T_{1RT} . Traditionally this has been done by partially deuterating CH_4 to, for instance CHD_3 , which dramatically reduces the dipole-dipole contribution. However, this has the drawback of turning a spherical molecule (CH_4) with one principle moment of inertia, into a symmetric-top molecule (CHD_3) with two principle moments of inertia. The theory of spin-rotation relaxation for symmetric-top molecules is much more complex than for spherical molecules, thereby making comparisons with measurements more complex.

MD (molecular dynamics) simulations provide an ideal tool for separating ^1H NMR relaxation mechanisms. As already shown for liquid-state n -alkanes in Ref. [35], MD simulations can naturally separate *intramolecular* T_{1R} from *intermolecular* T_{1T} ^1H - ^1H dipole-dipole relaxation, without deuteration, and without any adjustable parameters in the interpretation of the simulations. Such simulations yield unique insights into (a) the relative strengths of *intramolecular* versus *intermolecular* relaxation, (b)

* ps41@rice.edu

† dna6@rice.edu

the influence of internal motions on the molecular dynamics of non-rigid molecules, and (c) the validity of traditional hard-sphere models [36, 37] for different molecular geometries.

In this report we simulate spin-rotation relaxation. In Section II A, we develop a technique to determine the autocorrelation function for angular-velocity $G_J(t)$ of non-rigid spherical molecules. In Section II B we interpret $G_J(t)$ to yield the spin-rotation relaxation using the kinetic model and the diffusion model. In Section III A we compare simulation versus measurement for spin-rotation relaxation and translational diffusion. In Section III B we compare and analyze the correlation times for the different relaxation mechanisms. In Section III C we propose a new kinetic model to account for Eq. 1.

II. METHODOLOGY

A. Molecular simulation

The MD simulations were performed using NAMD [38] version 2.11. Methane was modeled using the CHARMM General Force field (CGenFF) [39]. The protocol for setting-up the initial simulation configuration was exactly as before [35]. As before, we created the initial simulation system by packing N copies of the molecule into a cube of volume L^3 using the Packmol program [40]. The volume was chosen such that the number density N/V corresponds to the experimentally determined number density at the specified temperatures listed in Table I. The simulation approach for these systems using NAMD was as before [35].

The angular-velocity computation went as follows. From simulations, for each atom in a molecule, we have a site velocity \mathbf{v}_i . Without loss of generality, we assume \mathbf{v}_i is relative to the velocity of the center of mass. By the definition of angular velocity, we have

$$\boldsymbol{\omega} \times \mathbf{r}_i = \mathbf{v}_i. \quad (2)$$

But a direct application of the above equation cannot be used to calculate $\boldsymbol{\omega}$ because the matrix equation is singular. We therefore define

$$\mathcal{L} = \sum_i |\mathbf{v}_i - \boldsymbol{\omega} \times \mathbf{r}_i|^2. \quad (3)$$

We minimize \mathcal{L} with respect to the x, y, z -components of $\boldsymbol{\omega}$, giving the following matrix equation:

$$\begin{pmatrix} \sum_i z_i^2 + y_i^2 & -\sum_i x_i y_i & -\sum_i x_i z_i \\ -\sum_i x_i y_i & \sum_i x_i^2 + z_i^2 & -\sum_i y_i z_i \\ -\sum_i x_i z_i & -\sum_i y_i z_i & \sum_i x_i^2 + y_i^2 \end{pmatrix} \begin{pmatrix} \omega_x \\ \omega_y \\ \omega_z \end{pmatrix} = \begin{pmatrix} \sum_i (\mathbf{r}_i \times \mathbf{v}_i)_x \\ \sum_i (\mathbf{r}_i \times \mathbf{v}_i)_y \\ \sum_i (\mathbf{r}_i \times \mathbf{v}_i)_z \end{pmatrix} \quad (4)$$

In tensor notation, we can write this more compactly as

$$r_j \omega_p r_q \epsilon^{ljk} \epsilon_{pqk} = r_j v_k \epsilon_{jkl}, \quad (5)$$

summed over all sites.

We constructed the above matrix for each molecule and solved for $\omega_x, \omega_y, \omega_z$. This calculation is repeated for all the frames in the trajectory. Then we calculated the autocorrelation of each component. Since the system is isotropic, all the component relaxations are the same. The above calculation is repeated for other molecules and the results averaged.

Phase	T	P	ρ	D_T	T_1	η	L
	(K)	(bar)	(g/cm ³)	(10 ⁻⁹ m ² /s)	(s)	(cP)	(Å)
	pred.	meas.	pred.	meas.	meas.	pred.	
L	90.9	0.120	0.451	2.52	9.7	0.192	31.15
L	105.3	0.578	0.432	4.35	14.5	0.134	31.62
L	125.0	2.69	0.402	7.76	18.8	0.089	32.37
L	142.9	7.41	0.372	11.8	20.2	0.064	33.23
S	194.8	389.8	0.359	18.0	16.4	0.056	33.63
S	194.8	141.0	0.303	25.5	14.9	0.037	35.56
S	194.8	71.24	0.255	34.0	12.8	0.027	37.69
S	194.8	59.76	0.230	39.4	11.6	0.024	38.96
S	194.8	52.53	0.173	56.2	9.05	0.017	43.35
S	298.2	349.1	0.232	56.5	7.11	0.027	38.89
S	298.2	250.0	0.188	74.5	5.95	0.022	41.69
S	194.8	46.53	0.089	116.1	4.77	0.010	40.20
S	298.2	151.1	0.120	120.4	3.61	0.016	48.50
S	273.2	99.46	0.089	160	3.04	0.014	40.14
S	273.2	82.56	0.072	200	2.44	0.013	43.07
S	273.2	64.68	0.054	264	1.74	0.012	47.41
G	273.2	45.29	0.036	404	1.21	0.011	54.51
S	307.7	51.73	0.035	439	0.96	0.012	54.76

TABLE I. List of MD simulated state points, chosen to coincide with measured (meas.) methane data taken from Ref. [9–12], including phase (Liquid, Supercritical, or, Gas), temperature (T), pressure (P), density (ρ), translational diffusion (D_T), ¹H NMR relaxation time (T_1), viscosity (η), and MD cube size L , in order of increasing D_T . Predicted quantities (pred.) are taken from NIST database. Critical points for methane are $T_{cr} = 190.6$ K and $P_{cr} = 46$ bar.

The translational-diffusion coefficient D_T was derived in a similar fashion to Ref. [35]. The linear slope of the mean-squared displacement was computed in the interval between 5 ps \leftrightarrow 10 ps. The periodic-boundary correction term [41, 42] was derived using viscosity η and box size L , both listed in Table I. The correction term resulted in a 5 \leftrightarrow 10 % boost in diffusion coefficient.

B. Spin-rotation relaxation

The Hamiltonian for the spin-rotation interaction is given by the following [16–20]:

$$\mathcal{H}_J = \hbar \sum_{i=1}^4 \mathbf{I}_i \cdot \mathbf{C}_i \cdot \mathbf{J}. \quad (6)$$

\mathbf{I}_i are the four ^1H nuclear spins on the methane molecule. \mathbf{J} is the angular momentum of the molecule, which is related to the angular velocity $\boldsymbol{\omega}$ by the following $\hbar\mathbf{J} = I\boldsymbol{\omega}$, where $I = 5.33 \times 10^{-47} \text{ kg m}^2$ [43] is the moment of inertia for methane. The coupling tensor \mathbf{C} has two principle components C_\perp and C_\parallel , which are proportional to the magnetic field (per unit J) generated at a ^1H by rotations about an axis \perp (\parallel) to the C-H bond axis, respectively. The most practical formulation separates \mathcal{H}_J into a scalar component proportional to the average coupling constant $C_a = (2C_\perp + C_\parallel)/3$, and a tensor component proportional to the diagonal coupling constant $C_d = (C_\perp - C_\parallel)$. The accepted values of the coupling constants, and the ones used here, are [20]: $C_a/2\pi = 10.4 \pm 0.1 \text{ kHz}$, $C_d/2\pi = 18.5 \pm 0.5 \text{ kHz}$ (which are the experimentally determined quantities), from which the following can be inferred $C_\perp/2\pi = 16.6 \pm 0.3 \text{ kHz}$, $C_\parallel/2\pi = -1.9 \pm 0.2 \text{ kHz}$.

The expression for the autocorrelation function $G_J^{lk}(t)$ used to determine T_{1J} for liquids [2] and gases [3, 4, 6] can be summarized as follows (in units of s^{-2}):

$$G_J^{lk}(t) = \frac{I^2}{2\hbar^2} (C_a^2 \langle \omega_l(t+\tau) \omega_k(\tau) \rangle_\tau + \frac{2}{9} C_d^2 \sum_{m,n,o,p} \alpha_{l,m,n}^{k,o,p} \langle Y_2^m(t+\tau) \omega_m(t+\tau) Y_2^p(\tau) \omega_o(\tau) \rangle_\tau). \quad (7)$$

The first term in Eq. 7 is the scalar term, while the second term is the tensor term. The more general expression also includes a cross-term proportional to $C_a C_d$, however it reduces to zero for spherically-symmetric molecules such as methane. The terms $\omega_k(t)$ is the angular velocity around the k axis at time t , and $Y_2^m(t)$ is the spherical harmonic of rank 2 and order m at time t . $\alpha_{l,m,n}^{k,o,p}$ is composed of two sets of 3- j symbols defined in [2].

The tensor term greatly simplifies provided the rotational motion $Y_2^m(t)$ is independent of the angular velocity $\omega_k(t)$. In such cases the bracketed term separates as $\langle Y_2^m(t+\tau) Y_2^p(\tau) \rangle_\tau \langle \omega_m(t+\tau) \omega_o(\tau) \rangle_\tau$. Traditional theories state the following expressions for hard spheres:

$$\langle \omega_l(t+\tau) \omega_k(\tau) \rangle_\tau = \delta_{l,k} \frac{kT}{I} \exp(-t/\tau_J), \quad (8)$$

$$\langle Y_2^{l*}(t+\tau) Y_2^k(\tau) \rangle_\tau = \delta_{l,k} \exp(-t/\tau_R). \quad (9)$$

The angular-velocity autocorrelation function in Eq. 8 is derived from the Langevin model with “friction time” τ_J [44]. The orientation autocorrelation function in Eq. 9 is the Deybe model with rotational correlation-time τ_R [36]. The orientation and angular-velocity autocorrelations can be separated provided either $\tau_J \gg \tau_R$ (gases)

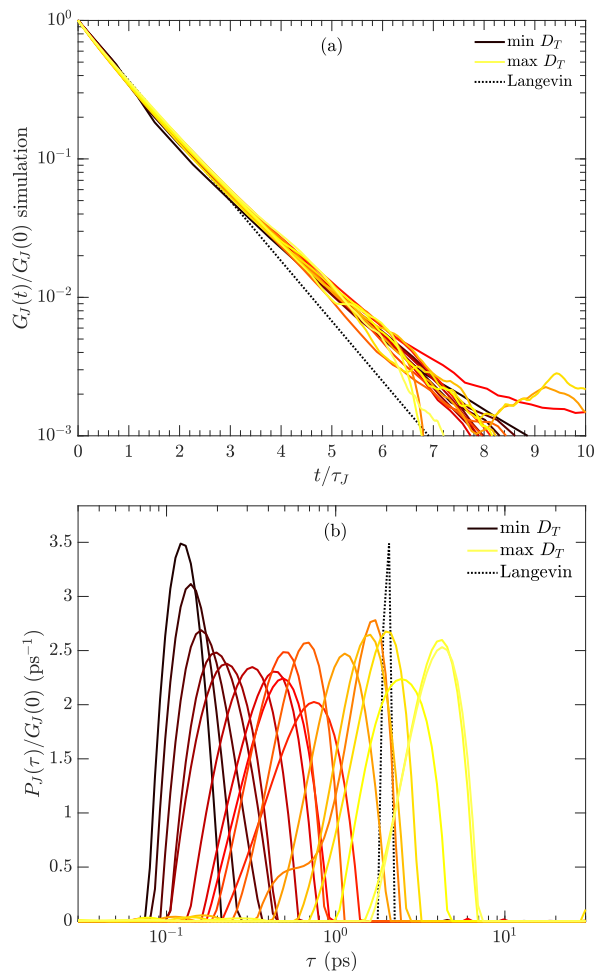


FIG. 1. (a) MD simulations of the autocorrelation function $G_J(t)$ for spin-rotation interactions using Eq. 10, colored in order of increasing D_T . The y -axis has been normalized by zero time value $G_J(0)$ in Eq. 11, and the x -axis has been normalized by correlation time τ_J in Eq. 14. The dotted line is Langevin prediction in Eq. 8. (b) Probability distribution function $P_J(\tau)$ of spin-rotational correlation time τ derived from the inverse Laplace transform (Eq. 20) of the $G_J(t)$ simulations in (a). Also shown is the Langevin prediction $G_J(t)$ from Eq. 8, generated with an arbitrarily chosen value of $\tau_J = 2 \text{ ps}$. The y -axis has been divided by $G_J(0)$, which normalizes the area of the distributions to unity (except for the Langevin model).

or $\tau_J \ll \tau_R$ (liquids) [2]. In the case of liquids ($\tau_J \ll \tau_R$), this has the effect of making $\langle Y_2^{l*}(t+\tau) Y_2^k(\tau) \rangle_\tau = \delta_{l,k}$ in Eq. 7. Based on comparison with measurements, the relation $\langle Y_2^{l*}(t+\tau) Y_2^k(\tau) \rangle_\tau = \delta_{l,k}$ is also used in the case of gases [6, 13, 15]. In such cases, Eq. 7 simplifies to the following expression which is used in the MD simulations:

$$G_J(t) = \frac{I^2}{2\hbar^2} (C_a^2 + \alpha_{\frac{2}{9}}^2 C_d^2) \langle \omega_k(t+\tau) \omega_k(\tau) \rangle_\tau \quad (10)$$

The resulting expression $G_J(t)$ is independent of the direction k in $G_J^{lk}(t)$, therefore the superscript is removed

for clarity. The MD simulations compute all three k directions independently, and the average is then taken to improve the signal to noise ratio. The simulation results for $G_J(t)$ are shown in Fig. 1(a), where both x and y axes have been normalized for better comparison of the functional form of the decay between the different states. The normalization also allows for comparison with the Langevin model in Eq. 8.

A significant parameter in the analysis is the autocorrelation at $t = 0$, which is given by the following expression:

$$G_J(0) = \frac{I^2}{2\hbar^2} (C_a^2 + \alpha \frac{2}{9} C_d^2) \langle \omega_k^2(\tau) \rangle_\tau = \frac{IkT}{2\hbar^2} (C_a^2 + \alpha \frac{2}{9} C_d^2) = \frac{1}{2} \Delta\omega_\alpha^2, \quad (11)$$

where the first equality is directly from Eq. 10. The second equality uses the time zero expression $\langle \omega_k^2(\tau) \rangle_\tau = kT/I$ from Eq. 8, which was verified from MD simulations to be within $\pm 1.5\%$ over the entire temperature range of interest. The third equality defines the second moment $\Delta\omega_\alpha^2$ (i.e. strength) of the spin-rotation interaction [45], given by:

$$\Delta\omega_{km}^2 = \frac{IkT}{\hbar^2} (C_a^2 + \frac{4}{45} C_d^2) \quad [\text{k.m.}, \alpha = \frac{2}{5}], \quad (12)$$

$$\Delta\omega_{dm}^2 = \frac{IkT}{\hbar^2} (C_a^2 + \frac{2}{9} C_d^2) \quad [\text{d.m.}, \alpha = 1]. \quad (13)$$

The only free parameter is α , which is given by $\alpha = 1$ in the diffusion model “ dm ” for liquids [2], or by $\alpha = 2/5$ in the kinetic model “ km ” for gases [6, 13]. In describing the kinetic model, we have adopted the exact relation for the scalar term $\hbar^2 \langle J(J+1) \rangle / 3 = IkT$, and for the tensor term we assume (without loss in accuracy) that $\langle (2J-1)(2J+3) \rangle / 4 \langle J(J+1) \rangle \simeq 1$ in the classical limit $J \gg 1$ [4]. The reason for $\alpha = 2/5$ in the kinetic model for gases is that the oscillatory terms $\Delta J \neq 0$ do not contribute (giving rise to $\times 1/5$), and from the statistical independence of $\omega_k(t)$ and $Y_2^m(t)$ (giving rise to $\times 2$) [4].

The next quantity of interest is the spin-rotation correlation time τ_J determined from the MD simulations, which is determined from the integral of the normalized $G_J(t)$ as such [45]:

$$\tau_J = \frac{1}{G_J(0)} \int_0^\infty G_J(t) dt. \quad (14)$$

The NMR relaxation times are then derived from the spectral density $J_J^\alpha(\omega)$ [2]:

$$J_J^\alpha(\omega) = 2 \int_0^\infty G_J(t) \cos(\omega t) dt, \quad (15)$$

$$\frac{1}{T_{1J}^\alpha} = 2J_J^\alpha(\omega_0),$$

$$\frac{1}{T_{2J}^\alpha} = J_J^\alpha(0) + J_J^\alpha(\omega_0),$$

where $\omega_0 = \gamma B_0$ is the Larmor frequency for ^1H . Given the short correlation times $\tau_J \sim 1$ ps, and given typical Larmor frequencies $\omega_0/2\pi < 500$ MHz, it is clearly the case that $\omega_0\tau_J \ll 1$, i.e. the fast-motion regime applies. In such cases $J_J^\alpha(0) = J_J^\alpha(\omega_0) = \Delta\omega_\alpha^2\tau_J$, and therefore $T_{1J}^\alpha = T_{2J}^\alpha$. Using the relation $1/T_{1J}^\alpha = 2J_J^\alpha(0) = 2\Delta\omega_\alpha^2\tau_J$ results in the final expressions:

$$\frac{1}{T_{1J}^{km}} = \frac{2IkT}{\hbar^2} (C_a^2 + \frac{4}{45} C_d^2) \tau_J, \quad (16)$$

$$\frac{1}{T_{1J}^{dm}} = \frac{2IkT}{\hbar^2} (C_a^2 + \frac{2}{9} C_d^2) \tau_J. \quad (17)$$

Note that T_{1J}^{dm} is often expressed in terms of C_\perp and C_\parallel instead [2], where $(C_a^2 + \frac{2}{9} C_d^2) = \frac{1}{3}(2C_\perp^2 + C_\parallel^2)$.

In order to compare with measurements, we also include contributions from the ^1H - ^1H dipole-dipole interactions, which separate into *intramolecular* T_{1R} and *intermolecular* T_{1T} relaxation. Details of the methodology behind the MD simulations of T_{1R} and T_{1T} can be found in Ref. [35]. The final expression for the total relaxation time is given by:

$$\frac{1}{T_1} = \frac{1}{T_{1R}} + \frac{1}{T_{1T}} + \frac{1}{T_{1J}^\alpha} = \frac{10}{3} \Delta\omega_R^2 \tau_{TR} + \frac{10}{3} \Delta\omega_T^2 \tau_{TT} + 2\Delta\omega_\alpha^2 \tau_J, \quad (18)$$

which takes on two different values T_{1J}^{km} and T_{1J}^{dm} , depending on the model T_{1J}^{km} and T_{1J}^{dm} used. $\Delta\omega_{R,T}^2$ and $\tau_{R,T}$ are the second-moments and correlation times for *intramolecular* (R) and *intermolecular* (T), respectively. For comparison purposes, the square-root of the second-moments at 298 K and 349.1 bar (for instance) are $\Delta\omega_R/2\pi \simeq 23.7$ kHz, $\Delta\omega_T/2\pi \simeq 7.5$ kHz, and $\Delta\omega_{J^{km}}/2\pi \simeq 51.8$ kHz. We also define the total relaxation from ^1H - ^1H dipole-dipole interactions T_{1RT} as such:

$$\frac{1}{T_{1RT}} = \frac{1}{T_{1R}} + \frac{1}{T_{1T}} \quad (19)$$

Given that the fast-motion regime applies, all of the above results for longitudinal relaxation T_1 apply equally to transverse relaxation T_2 . As such, the subscript 2 has been dropped everywhere for clarity.

1. Distribution in correlation times

As shown in Fig. 1(a), $G_J(t)$ deviates from single-exponential decay predicted by the Langevin model in Eq. 8. More specifically $G_J(t)$ has a more “stretched” (i.e. multi-exponential) decay, which we quantify by inverting the following Laplace transform [46, 47]:

$$G_J(t) = \int P_J(\tau) \exp(-t/\tau) d\tau \quad (20)$$

$P_J(\tau)$ (in units of s^{-3}) is the probability distribution function derived from the inversion. In the case of the

Langevin sphere model, $P_J(\tau)$ is a delta-function at τ_J , i.e. $P_J(\tau) = G_J(0) \delta(\tau - \tau_J)$. However, as shown in Fig. 1(a), $G_J(t)$ is always stretched (i.e. multi-exponential) to some degree, therefore $P_J(\tau)$ has a finite distribution. The decomposition of $G_J(t)$ into a sum of exponential decays is common practice [48], where the more complex the molecule dynamics, the more terms are required. This justifies our general approach of decomposing $G_J(t)$ into a “model free” sum of exponential decays in Eq. 20, for the purposes of quantifying the departure from the Langevin sphere model.

The resulting $P_J(\tau)$ distributions, shown in Fig. 1(b), were determined by using the discrete form of Eq. 20, using 100 logarithmically-spaced τ bins ranging from 0.03 ps $\leq \tau \leq$ 30 ps, and a fixed regularization parameter of 10^{-2} [46, 47]. Fig. 1(b) shows that the mean correlation-times τ_J get longer with increasing D_T , and that the width of the distributions get somewhat larger with increasing D_T . In all cases, the widths are much larger than the delta function prediction from the Langevin model in Eq. 8.

The widths of the $P_J(\tau)$ distributions were then quantified using the following:

$$\begin{aligned} \mu_J &= \frac{1}{G_J(0)} \int P_J(\tau) \ln(\tau) d\tau, \\ \sigma_J^2 &= \frac{1}{G_J(0)} \int P_J(\tau) (\ln(\tau) - \mu_J)^2 d\tau. \end{aligned} \quad (21)$$

σ_J is the standard deviation and μ_J is the mean of the variable $\ln(\tau)$. A natural logarithm in τ is used as the variable since the underlying $P_J(\tau)$ distributions are discrete and evenly spaced in $\ln(\tau)$. Also shown in Fig. 1(b) is the Langevin model which predicts $\sigma_J = 0$ (i.e. a delta function), or $\sigma_J \simeq 0.038$ due to regularization. Equivalent quantities were also derived for the intramolecular σ_R and intermolecular σ_T ^1H - ^1H dipole-dipole interactions.

III. RESULTS

A. Simulation versus measurement

The cross-plot of measured versus simulated translational-diffusion coefficient D_T in Fig. 2(a) indicates a strong correlation coefficient $R^2 = 0.996$, and an average absolute deviation of $\delta_{abs} = 9.2\%$, where δ_{abs} is defined as:

$$\delta_{abs} = \frac{1}{N} \sum_{i=1}^N \left| \frac{Y_i - X_i}{X_i} \right| \times 100. \quad (22)$$

Y_i are the simulated values, X_i are the measured quantities, and N is the number of points. The deviation is noticeable at the lowest temperature in the liquid phase ($T < T_{cr}$), which may be due to the proximity of the liquid-vapor phase transition, and/or temperatures are

low enough that nuclear quantum effects may be important (further investigations are beyond the scope of this work).

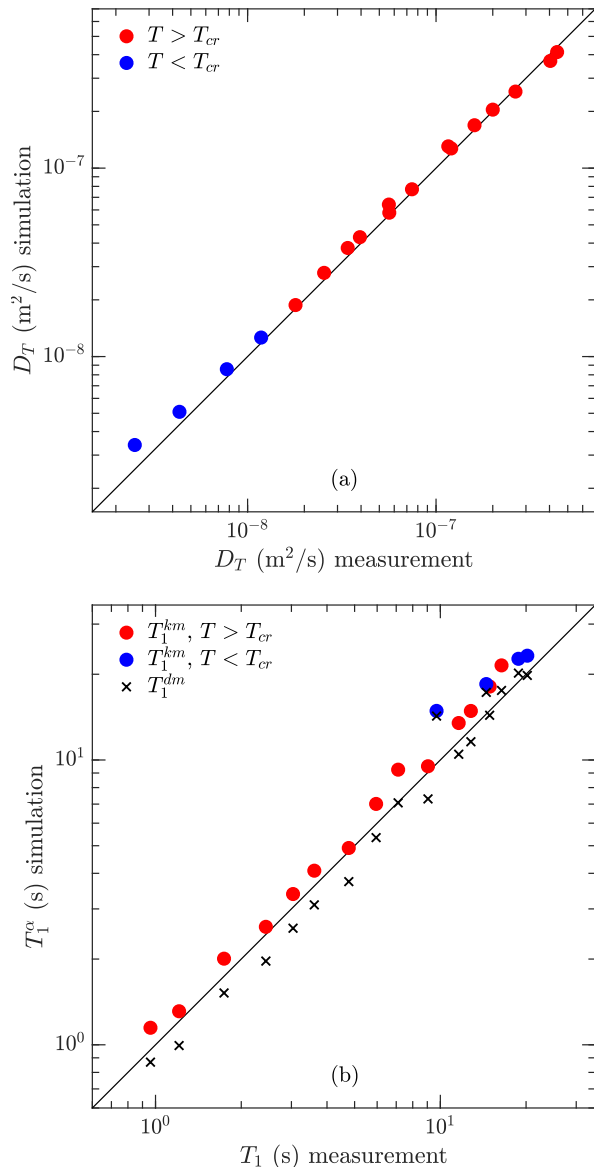


FIG. 2. (a) Cross-plot of simulated translational-diffusion coefficient D_T on the y -axis, versus measured D_T on the x -axis taken from Ref. [9–12], for both liquid state ($T < T_{cr}$), and supercritical or gas state ($T > T_{cr}$), listed in Table I. (b) Cross-plot of simulated total relaxation time T_1^α on the y -axis defined in Eq. 18, versus measured T_1 on the x -axis taken from Ref. [9–12], listed in Table I. The simulated T_1^α includes the kinetic model T_1^{km} and the diffusion model T_1^{dm} .

The cross-plot of measured T_1 versus simulated T_1^α (defined in Eq. 18) total-relaxation time in Fig. 2(b) indicates strong correlation coefficients of $R^2 = 0.982$ for T_1^{km} , and $R^2 = 0.954$ for T_1^{dm} , while δ_{abs} varies as a function of measured T_1 . At the higher D_T (i.e. lower ρ) end

where the measured $T_1 < 5$ s, the deviation is lower for the kinetic model T_1^{km} ($\delta_{abs} = 11.0\%$) than for the diffusion model T_1^{dm} ($\delta_{abs} = 15.8\%$). This is expected given that the kinetic model is more appropriate for fluids at high D_T and low ρ .

At the lower D_T (i.e. higher ρ) end where the measured $T_1 > 5$ s and $T > T_{cr}$ (i.e. still in the supercritical phase), the deviation is lower for the diffusion model T_1^{dm} ($\delta_{abs} = 8.6\%$) than for the kinetic model T_1^{km} ($\delta_{abs} = 19.7\%$). This is expected given that the diffusion model is more appropriate for fluids at low D_T and high ρ .

In the liquid phase where $T < T_{cr}$, ^1H - ^1H dipole-dipole relaxation begins to dominate over the spin-rotation interaction, and the two interpretations T_1^{km} and T_1^{dm} become comparable. Nevertheless, the deviation is still lower for the diffusion model T_1^{dm} ($\delta_{abs} = 18.9\%$) than for the kinetic model T_1^{km} ($\delta_{abs} = 29.1\%$). The source of the deviation is from the dipole-dipole contribution T_{1RT} , more specifically from the dominating *intermolecular* contribution T_{1T} . This systematic deviation is potentially due to the proximity of the liquid-vapor phase transition, and/or temperatures are low enough that nuclear quantum effects may be important (further investigations are beyond the scope of this work).

Another potential systematic error are the experimental uncertainties in the coupling constants C_a and C_d [20] listed in Section II. The maximum and minimum deviations reported in [20] result in a $\pm 2.7\%$ uncertainty in T_{1J}^{km} , and a $\pm 3.3\%$ uncertainty in T_{1J}^{dm} . These uncertainties are not insignificant in the above analysis, and should be taken into consideration when interpreting the simulations. There may also be uncertainty in the moment of inertia I for methane [43].

Yet another potential systematic error in the measurements is the presence of dissolved oxygen [49]. O_2 is paramagnetic, which would tend to shorten the measured T_1 compared to simulations. Given the large values of measured $T_1 \leq 20$ s, any trace amounts of oxygen could affect the results.

B. Correlation times

A summary of the simulated correlation times is shown in Fig. 3(a). The spin-rotation correlation time τ_J shows a monotonic increase with increasing D_T/T (translational-diffusion divided by absolute temperature). At high D_T/T , i.e. in the supercritical/gas phase ($T > T_{cr}$), τ_J is consistent with the kinetic collision time τ_K defined as:

$$D_T = \frac{1}{3}\lambda\bar{v}, \quad \bar{v} = \sqrt{\frac{8kT}{\pi M}}, \quad (23)$$

$$\tau_K = \frac{\lambda}{\bar{v}} = \frac{3D_T}{\bar{v}^2} = \frac{3\pi M}{8k} \frac{D_T}{T},$$

where $M = 2.664 \times 10^{-26}$ kg is the mass of the methane molecule, and \bar{v} is the mean thermal velocity. More

specifically, the correlation between τ_J and τ_K is strong $R^2 = 0.997$ and the absolute deviation is $\delta_{abs} = 7.7\%$ in this region. Given the compelling observation $\tau_J \simeq \tau_K$ and the relation $\tau_K \propto D_T/T$ in Eq. 23 motivates using D_T/T for the x -axis in Fig. 3. The relation $\tau_J \simeq \tau_K$ is indicative of the ‘‘strong collision’’ regime [4, 11], and is used below to infer a new relation for T_{1J}^{km} . As expected, the relation $\tau_J \simeq \tau_K$ breaks down in the liquid phase ($T < T_{cr}$) where the diffusion model is more appropriate.

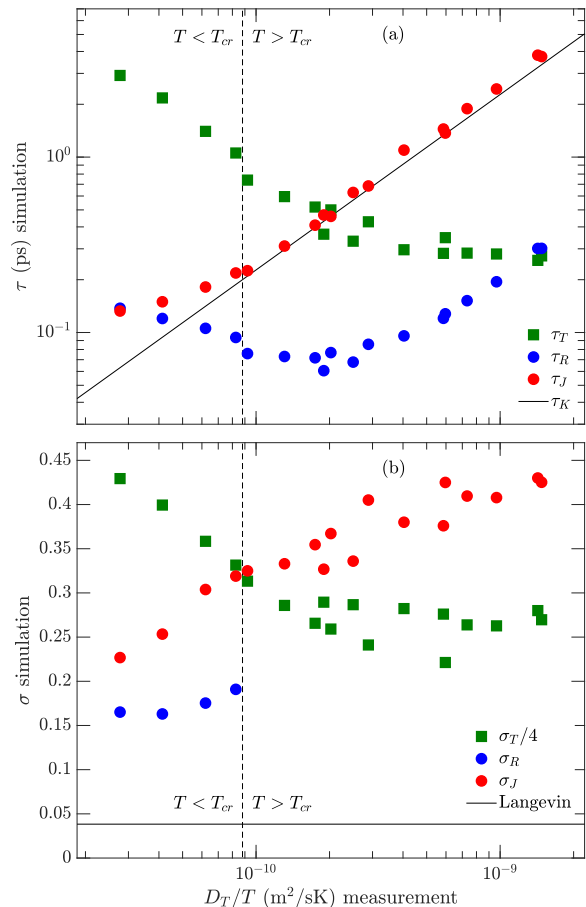


FIG. 3. (a) MD simulated correlation times for *intermolecular* τ_T and *intramolecular* τ_R ^1H - ^1H dipole-dipole interactions, spin-rotation interaction τ_J (Eq. 14), and mean collision time τ_K (Eq. 23), plotted against measured D_T/T . (b) Simulation results for the standard deviation σ_J (Eq. 21) in correlation times, determined from the $P_J(\tau)$ distributions (Eq. 20) in Fig. 1(b), plotted against measured D_T/T . Also shown is the Langevin model which predicts a delta function $\sigma_J = 0$, or $\sigma_J \simeq 0.038$ due to regularization. Equivalent quantities σ_R and σ_T for ^1H - ^1H dipole-dipole interactions are also shown, where $\sigma_T/4$ is plotted for clarity.

In the case of spherical molecules, the following simple theoretical predictions exist for relations between the *intramolecular* correlation time τ_R and spin-rotation cor-

relation time τ_J :

$$\tau_R = \frac{\tau_J}{2l+1} = \frac{\tau_J}{5} \quad [\text{k.m.}], \quad (24)$$

$$\tau_R \tau_J = \frac{I}{l(l+1)kT} = \frac{I}{6kT} \quad [\text{d.m.}]. \quad (25)$$

In the kinetic model ($T > T_{cr}$) for the supercritical/gas phase, Eq. 24 states that $\tau_R = \tau_J/5$ [4, 5], where $l = 2$ is the rank of rotational diffusion tensor for hard-spheres. As shown in Fig. 3(a) for $T > T_{cr}$, the relation $\tau_R \propto \tau_J$ is indeed found, however Eq. 24 overestimates τ_R by a factor $\simeq 2.5$. In the diffusion model ($T < T_{cr}$) for liquids, Eq. 25 [2] makes use of the Stokes-Einstein relation for hard-spheres, which predicts that rotational-diffusion $D_R = 1/l(l+1)\tau_R = 1/6\tau_R$ and translational-diffusion D_T are related by $D_T = 4a^2 D_R/3$ [2], where a is the methane radius. At the lowest D_T value the relation $\tau_R \propto 1/\tau_J$ is indeed found, however Eq. 25 underestimates τ_R by a factor $\simeq 2.5$.

In the liquid phase ($T < T_{cr}$), the intermolecular correlation time τ_T decreases with increasing D_T , in general accordance with the Stokes-Einstein relation for hard-spheres $\tau_D = \frac{5}{2}\tau_T = 2a^2/D_T$ [35]. A transport radius of $a \simeq 1.0 \text{ \AA}$ can be inferred at the lowest D_T value, which is consistent with the C-H internuclear distance of $a \simeq 1.093 \text{ \AA}$ deduced from the relation $I = \frac{8}{3}m_H a^2$ [43], where m_H is the ^1H mass. At high D_T , i.e. in the supercritical/gas phase ($T > T_{cr}$), the Stokes-Einstein relation breaks down, and τ_T becomes independent of D_T .

A summary of the simulated standard deviations σ in correlation-times is shown in Fig. 3(b). For spin-rotation, σ_J increases by a factor of two from the lowest D_T to the highest D_T , indicating a larger distribution in correlation times for the gas phase. In the case of intramolecular dipole-dipole, σ_R shows a low value in the liquid phase, and a possible increase with increasing D_T . In the supercritical/gas phase, $G_R(t)$ shows signs of oscillations at early times $t \lesssim 0.3$ ps, and then decays monotonically for $t \gtrsim 0.3$ ps. As such, σ_R is not computed for $T > T_{cr}$. Note that oscillations in $G_R(t)$ for $T > T_{cr}$ were previously predicted using the extended diffusion model [8, 14].

Meanwhile, σ_T decreases with increasing D_T , which is the opposite trend to σ_J and σ_R . At high D_T , σ_T plateaus to the $\sigma_T \simeq 1.25$ (note that Fig. 3(b) displays $\sigma_T/4$ for clarity), which is consistent with the inherent multi-exponential value of the Torrey hard-sphere model [37].

As stated in Eqs. 16 and 17, the longer the spin-rotation correlation-time τ_J , the shorter the relaxation time T_{1J} , i.e. the more significant the relaxation mechanism. The same is true for the ^1H - ^1H dipole-dipole mechanism [35]. It is therefore informative to compare the ratio of relaxation times between different mechanisms in order to determine which mechanism is dominant. Fig. 4(a) shows the ratio T_{1RT}/T_{1J}^{km} , where T_{1RT} is the total dipole-dipole relaxation defined in Eq. 19. A large

value $T_{1RT}/T_{1J}^{km} \gg 1$ indicates that spin-rotation dominates over dipole-dipole, as found at high D_T in the supercritical/gas phase ($T > T_{cr}$). Meanwhile a small value $T_{1RT}/T_{1J}^{km} \ll 1$ indicates that dipole-dipole dominates over spin-rotation, as found at low D_T in the liquid phase ($T < T_{cr}$).

A similar analysis can be made between the intramolecular and the intermolecular dipole-dipole interactions. A large value $T_{1T}/T_{1R} \gg 1$ indicates that intramolecular dominates over intermolecular, as found at high D_T in the supercritical/gas phase ($T > T_{cr}$). Meanwhile a small value $T_{1T}/T_{1R} \ll 1$ indicates that intermolecular dominates over intramolecular, as found at low D_T in the liquid phase ($T < T_{cr}$). The most likely reason for this is that $\tau_T \gg \tau_R$ in the liquid phase ($T < T_{cr}$). Meanwhile in the supercritical/gas phase ($T > T_{cr}$), even though $\tau_T \simeq \tau_R$, the intermolecular second-moment $\Delta\omega_T^2 \propto \rho$ [35], and therefore $\Delta\omega_T^2$ decreases with increasing D_T (i.e. decreasing ρ).

C. New Kinetic model

Building on the observation that $\tau_J \simeq \tau_K$ in the supercritical/gas phase ($T > T_{cr}$) (see Fig. 3(a)), and the observation that spin-rotation dominates over dipole-dipole $T_{1RT}/T_{1J}^{km} \gg 1$ in this region (Fig. 4(b)), it is informative to infer a new relation for $T_{1J}^{km} \simeq T_{1J}^{km}$ in the supercritical/gas phase. Assuming $\tau_J = \tau_K$ in Eq. 16, and using the definition for τ_K in Eq. 23 results in the following prediction:

$$\frac{1}{T_{1J}^K} = \frac{3\pi IM}{4\hbar^2} (C_a^2 + \frac{4}{45}C_d^2) D_T \quad [\text{k.m.}]. \quad (26)$$

The new prediction in the kinetic regime T_{1J}^K is plotted in Fig. 4(b) against the simulated T_{1J}^{km} and the measured D_T . In the supercritical/gas phase ($T > T_{cr}$), the correlation coefficient between T_{1J}^{km} and T_{1J}^K is found to be $R^2 = 0.998$, and the absolute deviation is found to be $\delta_{abs} = 7.7 \%$, without any adjustable parameters in the derivation of T_{1J}^K in Eq. 26. Moreover, there are no assumptions about an effective molecular radius. In the liquid phase ($T < T_{cr}$), T_{1J}^{km} starts to deviate from the kinetic model T_{1J}^K , as expected. Likewise, the total relaxation T_{1J}^{km} deviates from T_{1J}^K due to the T_{1RT} contribution, as expected.

Also shown in Fig. 4(b) is the empirical relation T_{1J}^A from Eq. 1, where $A = 6.37 \times 10^{-6}$ [22] in units of temperature T (K), density ρ (g/cm³), and T_{1J}^A (s). In the supercritical/gas phase ($T > T_{cr}$), the correlation between T_{1J}^A and T_{1J}^K is strong $R^2 = 0.957$, while the absolute deviation is $\delta_{abs} \simeq 21.2 \%$, for possibly the same reasons as discussed in Section III A. Eq. 1 and Eq. 8 imply that the T and ρ dependence of T_{1J} comes entirely from $D_T \propto T^{3/2}/\rho$. This is confirmed in the supercritical/gas phase ($T > T_{cr}$), where the correlation coefficient between measured D_T and measured $T^{3/2}/\rho$ in Table I is strong $R^2 = 0.991$.

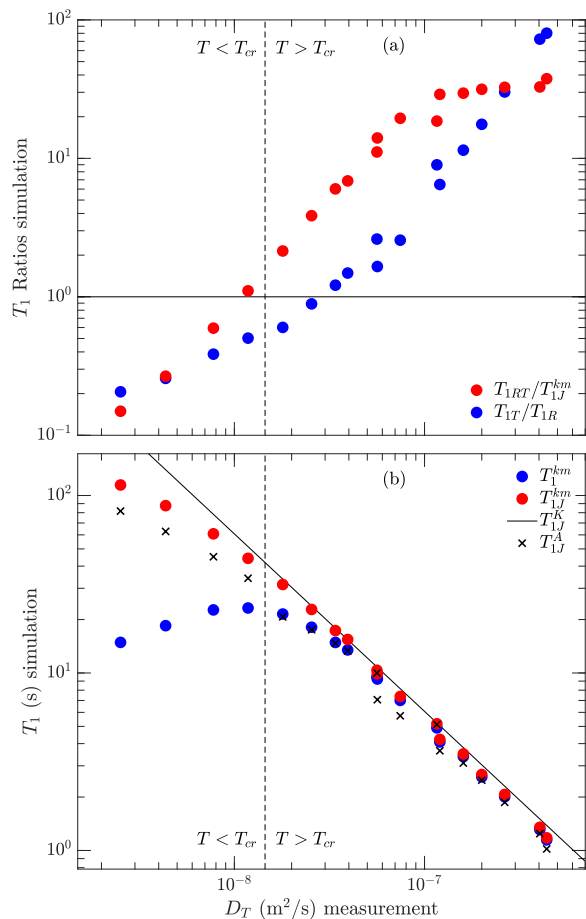


FIG. 4. (a) Ratio of simulated T_1 relaxation times to display relative strengths of the interactions; including, ratio of total dipole-dipole T_{1RT} (Eq. 19) to spin-rotation T_{1J}^{km} (Eq. 16), and ratio of *intermolecular* dipole-dipole T_{1T} to *intramolecular* dipole-dipole T_{1R} , plotted against measured D_T . (b) Simulated spin-rotation relaxation time T_{1J}^{km} (Eq. 16), empirical expression T_{1J}^A (Eq. 1), new prediction T_{1J}^K (Eq. 26), and total relaxation time T_1^{km} (Eq. 18), plotted against measured D_T .

IV. CONCLUSIONS

We develop a minimization technique to compute the angular-velocity for non-rigid spherical molecules, which is used to simulate the autocorrelation function $G_J(t)$ for the spin-rotation interaction of methane, over a wide range of densities ρ and temperatures T , spanning the liquid ($T < T_{cr}$), and supercritical/gas ($T > T_{cr}$) phases. The Langevin model predicts that $G_J(t)$ should decay with a single-exponential function with correlation time τ_J . However, inverse Laplace transforms of $G_J(t)$ indicate

a distribution in correlation times τ , with a standard deviation σ_J (i.e. width) which increases with increasing D_T (i.e. decreasing ρ).

T_{1J}^α is derived from $G_J(t)$ using the kinetic model “*km*” for gases (T_{1J}^{km}) [4], and the diffusion model “*dm*” for liquids (T_{1J}^{dm}) [2]. The total relaxation time T_1^{km} shows better agreement with measurements for $T_1 < 5$ s, with an absolute deviation of $\delta_{abs} = 11.0\%$ in this region. T_1^{dm} shows better agreement with measurements for $T_1 > 5$ s (and $T > T_{cr}$), with an absolute deviation of $\delta_{abs} = 8.6\%$ in this region. Uncertainties in the measured spin-rotation coupling-constants may contribute to these deviations. Meanwhile the simulated D_T agree well with measurements, without any adjustable parameters in the interpretation of the simulations.

MD simulations of the *intramolecular* and *intermolecular* ^1H - ^1H dipole-dipole relaxation are computed at the same state-points. T_{1J}^{km} is shown to dominate over the total dipole-dipole relaxation T_{1RT} at high D_T , while the opposite is found at low D_T .

The predicted relations between the *intramolecular* correlation-time τ_R and the spin-rotation correlation-time τ_J is tested, both in the liquid ($T < T_{cr}$) and the supercritical/gas phase ($T > T_{cr}$). At the highest D_T in the supercritical/gas phase, the relation $\tau_R = \tau_J/5$ [4, 5] is found to hold within a factor $\simeq 2.5$. At the lowest D_T in the liquid phase, the relation $\tau_R\tau_J = I/6kT$ [2] is also found to hold within a factor $\simeq 2.5$.

In the supercritical/gas phase ($T > T_{cr}$), τ_J is found to agree with the kinetic collision time τ_K , with an absolute deviation of $\delta_{abs} = 7.7\%$ in this region. Given this compelling finding, a new expression for the spin-rotation relaxation $1/T_{1J}^K \propto D_T$ is inferred without any adjustable parameters, and shows a strong correlation $R^2 = 0.957$ with the previously reported empirical finding $1/T_{1J}^A \propto T^{3/2}/\rho$.

ACKNOWLEDGMENTS

This work was funded by the Rice University Consortium on Processes in Porous Media, and the American Chemical Society Petroleum Research Fund [ACS-PRF-58859-ND6]. We gratefully acknowledge the National Energy Research Scientific Computing Center, which is supported by the Office of Science of the U.S. Department of Energy [DE-AC02-05CH11231], for HPC time and support. We also gratefully acknowledge the Texas Advanced Computing Center (TACC) at The University of Texas at Austin (URL: <http://www.tacc.utexas.edu>) for providing HPC resources, and Zeliang Chen for his assistance.

[1] H. S. Gutowsky, I. J. Lawrenson, K. Shimomura, Nuclear magnetic spin-lattice relaxation by spin-rotational inter-

actions, Physical Review Letters 6 (7) (1961) 349–351.

- [2] P. S. Hubbard, Theory of nuclear magnetic relaxation by spin-rotational interactions in liquids, *Phys. Rev.* 131 (3) (1963) 1155–1165.
- [3] M. Bloom, R. Dorothy, Determination of the spin-rotation interaction constants in CH_4 by means of nuclear spin relaxation measurements, *Can. J. Phys.* 45 (1967) 3411–3413.
- [4] M. Bloom, F. Bridges, W. N. Hardy, Nuclear spin relaxation in gaseous methane and its deuterated modifications, *Can. J. Phys.* 45 (1967) 3533–3554.
- [5] R. E. D. McClung, Rotational diffusion of spherical-top molecules in liquids, *J. Chem. Phys.* 51 (1969) 3842–3852.
- [6] R. Y. Dong, M. Bloom, Determination of spin-rotation interaction constants in fluorinated methane molecules by means of nuclear spin relaxation measurements, *Can. J. Phys.* 48 (1970) 793–804.
- [7] R. P. Dawson, F. Khoury, R. Kobayashi, Self-diffusion measured in methane by pulsed nuclear magnetic resonance, *AIChE J.* 16 (5) (1970) 725–729.
- [8] R. E. D. McClung, Rotational diffusion of spherical-top molecules in liquids. II. reorientation in liquid methane and solutions of methane in liquid noble gases, *J. Chem. Phys.* 55 (7) (1971) 3459–3467.
- [9] C. J. Gerritsma, N. J. Trappeniers, Proton-spin-lattice relaxation and self diffusion in methanes, I. spin-echo spectrometer and preparation of the methane samples, *Physica* 51 (1971) 365–380.
- [10] C. J. Gerritsma, P. H. Oosting, N. J. Trappeniers, Proton-spin-lattice relaxation and self diffusion in methanes, II. experimental results for proton-spin-lattice relaxation times, *Physica* 51 (1971) 381–394.
- [11] P. H. Oosting, N. J. Trappeniers, Proton-spin-lattice relaxation and self diffusion in methanes, III. interpretation of proton-spin-lattice experiments, *Physica* 51 (1971) 395–417.
- [12] P. H. Oosting, N. J. Trappeniers, Proton-spin-lattice relaxation and self diffusion in methanes, IV. self-diffusion in methane, *Physica* 51 (1971) 418–431.
- [13] S. Rajan, K. Lalita, S. V. Babu, Nuclear spin-lattice relaxation in CH_4 -inert gas mixtures, *J. Magn. Reson.* 16 (1974) 115–129.
- [14] R. E. D. McClung, On the extended rotational diffusion model for molecular reorientation in fluids, *Adv. Mol. Relax. Interact. Processes* 10 (1977) 83–171.
- [15] R. E. D. McClung, Spin-rotation relaxation theory, *eMagRes* DOI: 10.1002/9780470034590.emrstm0524.
- [16] J. W. Cederberg, C. H. Anderson, N. F. Ramsey, Rotational magnetic moments, *Phys. Rev.* 136 (4A) (1964) 960–961.
- [17] C. H. Anderson, N. F. Ramsey, Magnetic resonance molecular-beam spectra of methane, *Phys. Rev.* 149 (1) (1966) 14–24.
- [18] P.-N. Yi, I. Ozier, C. H. Anderson, Theory of nuclear hyperfine interactions in spherical-top molecules, *Phys. Rev.* 165 (1) (1968) 92–109.
- [19] I. Ozier, L. M. Crapo, S. S. Lee, Nuclear radio-frequency spectra of a series of tetrahedral molecules, *Phys. Rev.* 172 (1968) 63–82.
- [20] P.-N. Yi, I. Ozier, C. H. Anderson, Low-field hyperfine spectrum of CH_4 , *J. Chem. Phys.* 55 (11) (1971) 5215–5227.
- [21] Y. Zhang, G. J. Hirasaki, W. V. House, R. Kobayashi, Oil and gas NMR properties: the light and heavy ends, *Soc. Petrophys. Well Log Analysts* (2002) SPWLA–2002–HHH.
- [22] S.-W. Lo, G. J. Hirasaki, W. V. House, R. Kobayashi, Mixing rules and correlations of NMR relaxation time with viscosity, diffusivity, and gas/oil ratio of methane/hydrocarbon mixtures, *Soc. Petrol. Eng. J.* 7 (1) (2002) 24–34.
- [23] M. D. Hürlimann, D. E. Freed, L. J. Zielinski, Y.-Q. Song, G. Leu, C. Straley, C. C. Minh, A. Boyd, Hydrocarbon composition from NMR diffusion and relaxation data, *Petrophysics* 50 (2) (2009) 116–129.
- [24] Z. Yang, G. J. Hirasaki, M. Appel, D. A. Reed, Viscosity evaluation for NMR well logging of live heavy oils, *Petrophysics* 53 (1) (2012) 22–37.
- [25] C. Straley, An experimental investigation of methane in rock materials, *Soc. Petrophys. Well Log Analysts* (1997) SPWLA–1997–AA.
- [26] R. F. Sigal, E. Odusina, Laboratory NMR measurements on methane saturated barnett shale samples, *Petrophysics* 52 (1) (2011) 32–49.
- [27] R. Kausik, C.-C. Minh, L. Zielinski, B. Vissapragada, R. Akkurt, Y.-Q. Song, C. Liu, S. Jones, E. Blair, Characterization of gas dynamics in kerogen nanopores by NMR, *Soc. Petrol. Eng. SPE-147198-MS*.
- [28] A. Tinni, E. Odusina, I. Sulucarnain, C. Sondergeld, C. Rai, NMR response of brine, oil, and methane in organic rich shales, *Soc. Petrol. Eng.* (2014) SPE–168971–MS.
- [29] H.-J. Wang, A. Mutina, R. Kausik, High-field nuclear magnetic resonance observation of gas shale fracturing by methane gas, *Energy Fuels* 28 (2014) 3638–3644.
- [30] A. Papaioannou, R. Kausik, Methane storage in nanoporous media as observed via high-field NMR relaxometry, *Phys. Rev. Applied* 4 (2) (2015) 024018, 1–11.
- [31] R. F. Sigal, Pore-size distribution for organic-shale-reservoir rocks from nuclear-magnetic-resonance spectra combined with adsorption measurements, *Soc. Petrol. Eng. J.* 20 (4) (2015) 824–830.
- [32] R. Kausik, K. Fella, E. Rylander, P. M. Singer, R. E. Lewis, S. M. Sinclair, NMR relaxometry in shale and implications on logging, *Petrophysics* 57 (4) (2016) 339–350.
- [33] A. Valori, S. V. den Berg, F. Ali, W. Abdallah, Permeability estimation from NMR time dependent methane saturation monitoring in shales, *Energy Fuels* 31 (2017) 5913–5925.
- [34] A. Tinni, C. Sondergeld, C. Rai, New perspectives on the effects of gas adsorption on storage and production of natural gas from shale formations, *Petrophysics* 59 (1) (2018) 99–104.
- [35] P. M. Singer, D. Asthagiri, W. G. Chapman, G. J. Hirasaki, Molecular dynamics simulations of NMR relaxation and diffusion of bulk hydrocarbons and water, *J. Magn. Reson.* 277 (2017) 15–24.
- [36] N. Bloembergen, E. M. Purcell, R. V. Pound, Relaxation effects in nuclear magnetic resonance absorption, *Phys. Rev.* 73 (7) (1948) 679–712.
- [37] H. C. Torrey, Nuclear spin relaxation by translational diffusion, *Phys. Rev.* 92 (4) (1953) 962–969.
- [38] J. C. Phillips, R. Braun, W. Wang, E. Tajkhorshid, E. Villa, C. Chipot, R. Skeel, L. Kale, K. Schulten, Scalable molecular dynamics with NAMD, *J. Comput. Chem.* 26 (2005) 1781–1802.
- [39] K. Vanommeslaeghe, E. Hatcher, C. Acharya, S. Kundu, S. Zhong, J. Shim, E. Darian, O. Guvench, P. Lopes,

- I. Vorobyov, A. D. M. Jr., CHARMM general force field: A force field for drug-like molecules compatible with the CHARMM all-atom additive biological force field, *J. Comput. Chem.* 31 (2010) 671–690.
- [40] L. Martinez, R. Andrade, E. G. Birgin, J. M. Martinez, Packmol: A package for building initial configuration for molecular dynamics simulations, *J. Comput. Chem.* 30 (2009) 2157–2164.
- [41] I.-C. Yeh, G. Hummer, System-size dependence of diffusion coefficients and viscosities from molecular dynamics simulations with periodic boundary conditions, *J. Phys. Chem. B* 108 (2004) 15873–15879.
- [42] B. Dünweg, K. Kremer, Molecular dynamics simulation of a polymer chain in solution, *J. Chem. Phys.* 99 (1993) 6983–6997.
- [43] G. Herzberg, *Infrared and Raman Spectra of Polyatomic Molecules*, D. Van Nostrand Company, Inc. , New York, 1945.
- [44] J. McConnell, *The Theory of Nuclear Magnetic Relaxation in Liquids*, Cambridge University Press, 1987.
- [45] B. Cowan, *Nuclear Magnetic Resonance and Relaxation*, Cambridge University Press, 1997.
- [46] L. Venkataramanan, Y.-Q. Song, M. D. Hürlimann, Solving fredholm integrals of the first kind with tensor product structure in 2 and 2.5 dimensions, *IEEE Transactions on Signal Processing* 50 (5) (2002) 1017–1026.
- [47] Y.-Q. Song, L. Venkataramanan, M. D. Hürlimann, M. Flaum, P. Frulla, C. Straley, T_1 - T_2 correlation spectra obtained using fast two-dimensional laplace inversion, *J. Magn. Reson.* 154 (2002) 261–268.
- [48] P. A. Beckmann, Spectral densities and nuclear spin relaxation in solids, *Phys. Rep.* 171 (3) (1988) 85–128.
- [49] I. Shikhov, C. Arns, Temperature-dependent oxygen effect on NMR D - T_2 relaxation-diffusion correlation of n -alkanes, *Appl. Magn. Reson.* 47 (12) (2016) 1391–1408.